ACS APPLIED MATERIALS & INTERFACES

www.acsami.org

Research Article

Electrochemical Stability of Thiolate Self-Assembled Monolayers on Au, Pt, and Cu

Nathanael C. Ramos, J. Will Medlin,* and Adam Holewinski*

Cite This: *ACS Appl. Mater. Interfaces* 2023, 15, 14470−14480

Read Online

ACCESS | Metrics & More | Article Recommendations | Supporting Information

ABSTRACT: Self-assembled monolayers (SAMs) of thiolates have increasingly been used for modification of metal surfaces in electrochemical applications including selective catalysis (e.g., CO_2 reduction, nitrogen reduction) and chemical sensing. Here, the stable electrochemical potential window of thiolate SAMs on Au, Pt, and Cu electrodes is systematically studied for a variety of thiols in aqueous electrolyte systems. For fixed tail-group functionality, the reductive stability of thiolate SAMs is found to follow the trend Au < Pt < Cu; this can be understood by considering the combined influences of the binding strength of sulfur and competitive adsorption of hydrogen. The oxidative stability of thiolate SAMs is found to follow the order: Cu < Pt < Au, consistent with each surface's propensity toward surface oxide formation. The stable reductive and oxidative potential limits are both found to vary linearly with pH, except for reduction above pH ∼10, which is independent of pH for most thiol compositions. The electrochemical stability across different functionalized thiols is then revealed to depend on many different factors including SAM defects (accessible surface metal atom sites decrease stability), intermolecular interactions (hydrophilic groups reduce the stability), and SAM thickness (stability increases with alkanethiol carbon chain length) as well as factors such as SAM-induced surface reconstruction and the ability to directly oxidize or reduce the non-sulfur part of the SAM molecule.

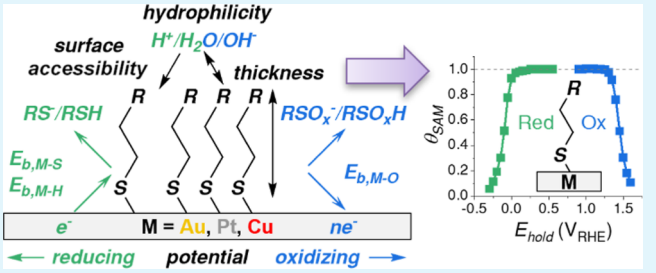

KEYWORDS: *self-assembled monolayer, electrochemical stability, reductive desorption, oxidative desorption, surface reconstruction, thiol, electrocatalysis*

1. INTRODUCTION

Self-assembled monolayers (SAMs) have been used to modify surfaces for a variety of applications. Different combinations of ligands and substrates produce different surface properties such as wettability, surface accessibility, surface chemistry, and surface electronic states. In catalysis applications, SAMs can provide stabilization of intermediates and can direct reactants to specific active sites, emulating enzyme catalysis and influencing activity and selectivity.[1,2] For example, phenyl thiols coated on Pt/Al_2O_3 catalysts have been found to direct selective hydrogenation of cinnamaldehyde to cinnamyl alcohol through $\pi-\pi$ interactions between the reactant and the SAM.[3] Other recent studies have found that Au nanoparticles modified with thiolate capping ligands create a selectively permeable hydrophobic monolayer for the CO_2 reduction reaction (CO_2RR) and repel trace transition metal cations (which can poison the catalyst surface)[4] and water (which leads to hydrogen evolution, HER).[5] Nonetheless, the broader applicability of SAM-modified surfaces for catalysis and electrocatalysis is limited by the scarcity of established stability benchmarks under operating conditions.

While the stability of SAMs exposed to air, light, high temperatures, solvents, and reactive atmospheres has been extensively characterized,[6,7] the stability of SAMs in an electrochemical environment has been less studied. Most electrochemical studies of SAMs have focused on their reductive desorption from Au in basic electrolyte because this process occurs at potentials more positive than the HER (making it easily resolvable).[8] Salvarezza and co-workers recently compiled results for reductive desorption of thiolate SAMs on different single-crystal Au surfaces and concluded that the desorption potential best correlates with the standard Gibbs free energy of adsorption of the SAM, which accounts for the thiolate surface coverage, binding energy, and intermolecular interactions.[9] In comparison, another study found that thiolates are removed from Pt in basic electrolytes in the HER region at potentials more negative than for the same thiolates on Au.[10] In the case of Cu, one study found that alkanethiolate SAMs reductively desorb at potentials ∼600 mV more negative than on Au.[11] In contrast to reductive desorption, the oxidative stability of thiolate SAMs on

Received: January 26, 2023
Accepted: February 28, 2023
Published: March 10, 2023

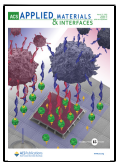

common metal electrodes has not been systematically studied. Based on the cyclic voltammetry behavior of alkanethiolate monolayers on Au, Porter and co-workers[8] proposed that whereas the reductive desorption of thiolate SAMs is likely via one electron transfer, oxidative removal could involve three electron transfers. Knowledge of these processes and the stable potential window is essential for identifying the range of applicability for influencing reactions including CO_2RR, HER, oxygen evolution reaction (OER), and oxygen reduction reaction (ORR), among others.

In this paper, we systematically investigate the electrochemical stability of thiolate SAMs on polycrystalline Au, Pt, and Cu in aqueous electrolytes. Whereas prior studies have focused heavily on alkane or aromatic thiols, reductive desorption, and Au electrodes, here we explore the effects of additional chemical functionalities for both oxidation and reduction as a function of pH on each of three common electrode materials. The stable electrochemical potential window is established for each metal-thiol-electrolyte system, and the collective trends are discussed to propose a more generalized understanding of contributions to the electrochemical stability of SAMs.

2. EXPERIMENTAL SECTION

2.1. Materials and Chemicals. All chemicals were used as purchased without further purification. SAM deposition solutions were formed from 1-propanethiol (C3, 99%, Aldrich), 1-hexanethiol (C6, 95%, Fluka), 1-decanethiol (C10, 96%, Alfa Aesar), 1-adamantanethiol (ADT, 95%, Aldrich), thioglycerol (TG, >99%, Sigma), 2-mercaptopropionic acid or thiolactic acid (TLA, 95%, Aldrich), 3-mercapto-1-propanol (3-MPOL, 95%, Aldrich), 3-mercaptopropionic acid (3-MPA, >99%, Aldrich), cysteamine (CYST, 95%, Aldrich), thiophenol (TP, >99%, Aldrich), benzyl mercaptan (BZT, 99%, Aldrich), 4-mercaptopyridine (4-MPyS, 95%, Sigma-Aldrich), or 3-chloro-1-propanethiol (3-Cl, 98%, Aldrich) in ethanol (200 proof, 100%, Decon Labs). All electrolytes were prepared in ultrapure deionized water (>18.2 MΩ cm, Millipore) with Suprapur $HClO_4$ (Sigma-Aldrich, 99.999%), $NaHCO_3$ (Sigma-Aldrich, >99.7%), NaH_2PO_4 (Acros, 99%), Na_2HPO_4 (Aldrich, 99.95%), Na_2CO_3 (Fisher, >99.5%), or KOH (Aldrich, 99.99%) and purged of oxygen with argon (UHP, AirGas). H_3PO_4 (ACS Reagent, Sigma-Aldrich, 85%) was used for the pretreatment of Cu.

Au foil (99.99%, 0.25 mm thick, Goodfellow), Au wire (99.95%, 0.75 mm diameter, Goodfellow), Pt foil (99.99%, 0.25 mm thick, Goodfellow), Pt wire (99.99%, 0.8 mm diameter, Goodfellow), Cu foil (99.9999%, 0.25 mm thick, Thermo Fisher), Cu wire (99.9999%, 1 mm diameter, Thermo Fisher), and graphite foil (99.8%, 0.5 mm thick, Alfa Aesar) electrodes were used.

2.2. Electrode Preparation and Characterization. Electrochemical experiments were conducted using a Biologic Potentiostat SP-300 with a typical three-electrode cell setup. The working electrodes were Au, Pt, or Cu wire. The counter electrodes in each experiment were larger surface area Au, Pt, or graphite plates, respectively. All experiments used a Ag/AgCl reference electrode (sat'd KCl); the reference potential was measured to be 0.197 V versus NHE. All experiments were conducted in an aqueous electrolyte saturated with argon unless otherwise noted.

Au was electrochemically polished using cyclic voltammetry in 0.1 M $HClO_4$ for 30 cycles between 0.1 and 1.7 V versus RHE at 300 mV/s. An electrode profile was taken in the same potential window at 100 mV/s and used to determine the electrochemically active area (ECSA) from the gold oxide reduction peak with a conversion factor of 386 $\mu C/cm^2$.[12] This area, before deposition of the SAM, is the normalization factor for the current reported on Au in cyclic voltammograms (CVs) and linear sweep voltammograms (LSVs), as well as double layer capacitance (C), throughout the paper and Supporting Information.

Pt was flame-cleaned and subsequently electrochemically polished using cyclic voltammetry in 0.1 M $HClO_4$ for 30 cycles between 0.1 and 1.4 V versus RHE at 300 mV/s. An electrode profile was taken in the same potential window at 100 mV/s and used to determine the ECSA from the hydrogen underpotential deposition (H_{UPD}) charge with a conversion factor of 210 $\mu C/cm^2$.[13] This area, before deposition of the SAM, is the normalization factor for the current reported on Pt in CVs and LSVs, as well as C, throughout the paper and Supporting Information.

Cu was electropolished in 85% phosphoric acid for 1 min using a two-electrode setup with a Cu wire counter electrode. This has been shown to result in a very smooth surface.[14] Therefore, the geometric area of the Cu electrode is the normalization factor for the current reported on Cu in CVs and LSVs, as well as C, throughout the paper and Supporting Information.[15]

After electrochemically pretreating each electrode, C was measured in each case by fitting the double layer current measured at different scan rates (50, 100, 150, 200, 250, 300 mV/s) from CVs confined to the double layer potential window. Thiolate SAMs were prepared by soaking each electrode in an ethanol-thiol solution (1−5 mM) for 10 min, following standard procedures established in the literature.[16,17] This procedure formed full-coverage SAMs with comparable LSVs, contact angles, capacitances, and surface coverages compared to other works (for direct comparisons and associated plots, see the Supporting Information). In some cases, these SAMs may have lower crystallinity than if given longer time to equilibrate, but this should only lead to conservative estimates on their stability. Electrodes were then rinsed with ethanol, followed by water, and returned to the electrochemical cell. The capacitance of the SAM-coated electrode was again determined by cyclic voltammetry and used to estimate coverage as discussed further below. On Cu, the potential was held at −0.2 V versus RHE prior to C measurement to remove any surface oxide formed from air or water.

2.3. Thiolate SAM Electrochemical Stability Testing. Oxidative and reductive stability were assessed separately since bound thiolate molecules may be oxidatively or reductively transformed irreversibly and/or removed. For each process, the electrochemical stability window across different systems was investigated in two ways. First, CVs were taken to compare the electrochemical characteristics of the SAM-coated electrode to the uncoated electrode. Second, stability was compared more quantitatively using potential holds and C measurements. Starting at a stable potential, the potential was scanned at 100 mV/s to a more positive (to study oxidative stability) or negative (to study reductive stability) potential and held for 2 min and then scanned back to the starting potential. The double layer capacitance was then determined as described above to assess coverage changes. This procedure was repeated at successively more positive or negative potential limits in 50 mV increments. The potential sequence is summarized in Figure S1. X-ray photoelectron spectroscopy (XPS, Kratos Axis Supra) was further used on a subset of samples to validate the methodology of using capacitance to characterize the stability and coverage of SAMs (see Figure S2, associated methods, peak fits, and discussion in the Supporting Information). Contact angle measurements of 18 MΩ water on different SAM-metal surfaces were taken to verify SAM formation and degree of order within different alkanethiols (Figure S3). An ARTRAY:ARTCAM-130MI-BW camera was used, and contact angles were determined using the First Ten Angstroms contact angle software (FTA32, Portsmouth, VA) using an average of at least five different spots on each sample.

3. RESULTS AND DISCUSSION

3.1. General Voltammetric Features. SAMs formed from 1-propanethiol (C3) were first surveyed as model systems to compare general electrochemical features of adsorbed thiolates across metals. Basic conditions (0.1 M KOH) were chosen so that reductive desorption could be observed with less competition from HER. The electrochemical behavior of each C3/metal system was probed with cyclic voltammetry and

https://doi.org/10.1021/acsami.3c01224
ACS Appl. Mater. Interfaces 2023, 15, 14470−14480

is compared against each unmodified metal in Figure 1; these measurements agree with similar systems reported in the literature.[8,18,19]

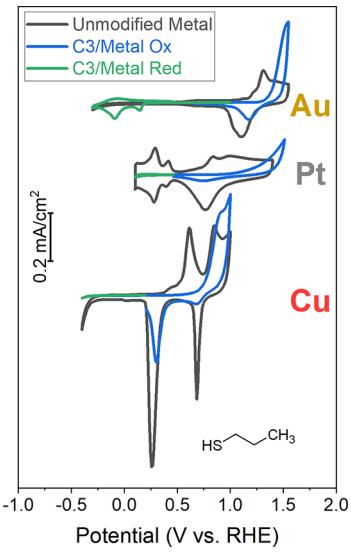

Figure 1. CVs at 100 mV/s showing desorption features of 1-propanethiol (C3) from Au, Pt, and Cu in 0.1 M KOH. Unmodified electrodes are shown in black. The first oxidative CV with C3 modification is shown in blue. The first reductive CV with C3 modification is shown in green.

In the top green trace of Figure 1, there are two clear peaks showing the reductive desorption of C3 from Au. These features are well known in the literature and have been attributed to C3 desorbing from different surface sites on polycrystalline Au.[20] During the reverse sweep, there is oxidative current associated with readsorption of a portion of the thiolates back onto the Au surface due to the low solubility of alkanethiolates in water and slow diffusion away from the electrode.[8] These desorption and readsorption processes have both been confirmed by in situ STM.[21,22] If some fraction of thiolates are readsorbed after the first CV cycle, successive CVs can show a shift in reductive desorption peak potential due to the loss of stabilizing intermolecular lateral interactions between thiolate molecules at sub-monolayer coverages (see Figure S4a).[23] In contrast to Au, the reductive CVs of Pt and Cu (second and third green traces in Figure 1) do not show any desorption peaks corresponding to C3 up to the onset of HER. For Pt and Cu, the SAM layer significantly delays HER onset due to strong chemisorption of the thiolates; blocking of the metal active sites leads to HER being initiated concurrently with the beginning of SAM removal. For Pt, there is also complete suppression of the characteristic hydrogen underpotential deposition (H_{UPD}) peaks prior to the HER window. C3 does not affect HER much on Au since the HER on bare Au occurs at potentials more negative than the onset of C3 desorption.

The oxidative desorption CVs of C3 for each metal (blue traces) are also shown in Figure 1. For the C3-modified electrodes, surface oxide formation is suppressed, but significant oxidative current appears toward the higher side of the surface oxidation voltage windows. This current most likely initiates with the oxidation of the SAM itself, giving way to surface oxide formation—this is evidenced by the presence of a small oxide reduction peak on the reverse sweep, a behavior seen previously for thiolate SAMs.[8] The assignment of the initial oxidation wave corresponding to thiolate oxidation (and removal)[24] has been confirmed by in situ STM measurements showing thiolate SAMs losing order and desorbing.[25] Sequential CVs of C3 on Au show that the SAM oxidation is irreversible, and after several cycles, the unmodified electrode character reappears (see Figure S4b). It has been proposed that SAMs mainly oxidize (irreversibly) to form RSO_2^-; this assignment has been based on charge passed from CVs,[8] XPS,[24] and in situ FTIR experiments on Au.[24,26]

3.2. Stability Trends with Metal. From cyclic voltammetry alone, it is generally difficult to identify when a SAM begins to desorb from a surface. This is especially the case for the reductive stability of SAMs on Pt and Cu, where desorption occurs in parallel to HER. Furthermore, it is impossible to differentiate between SAM oxidation and surface oxidation currents or to know what oxidation state the SO_x head group must reach before formally dissociating from the surface. Thus, the electrochemical stability of thiolate SAMs was assessed using double layer capacitance (C) measurements following a series of potential holds at increasingly oxidizing or reducing potentials.

To create a stability metric, C was measured for a series of two-minute potential holds to estimate the potential-dependent surface coverage of the SAM. The current, I, was measured in the double layer region at various scan rates, ν, and fit to a line ($I = C\nu$) to approximate C. The measured capacitance, C, was estimated to be a linear combination of the component attributed to the bare electrode, C_{bare}, and the component attributed to the full-density SAM, C_{full}

$$C = C_{full}\theta + C_{bare}(1 - \theta) \quad (1)$$

where θ is the fraction of a saturating monolayer (apparent surface coverage of SAM). Physically, this approximates that the desorption process leaves the surface with distinct regions of a saturating SAM and uncoated metal. Surface-bound thiolates are stabilized by intermolecular interactions; therefore, it is more energetically favorable for them to be bound closer together than homogeneously far apart.[27] This is consistent with the literature where desorption has been observed to propagate from defect sites instead of randomly or uniformly.[22] There is additional inherent uncertainty in defining coverage as a function of potential due to the discrete spacing of the potential holds and the fact that desorption may not fully equilibrate in 2 min. Sulfur adlayers may also modify capacitance if the C−S bond is cleaved during oxidation or reduction.[24,28] Nonetheless, we believe that the methodology is sufficient to gain a working definition of desorption "onset", which is otherwise ill-defined and timescale dependent.

Measured values of θ for C3 (according to Equation 1) are reported in Figure 2a for increasingly positive or negative potentials on Au, Pt, and Cu in 0.1 M KOH. The average value and error in θ at each hold potential are plotted based on two replicates. With decreasing θ, the uncertainty increases due to error compounding with each successive potential hold. Nevertheless, the error is low (less than the size of the data point) at less extreme potentials, where $\theta \sim 0.9-1.0$, validating the ability to reproducibly identify the potential where the SAM removal is initiated (i.e., where $\theta < 1.0$ is first encountered). XPS data for C3 on Au (Figure S2) validates the use of capacitance as a metric for thiolate coverage and confirms the origin of the redox peaks in Figure 1. Figure 2b

https://doi.org/10.1021/acsami.3c01224
ACS Appl. Mater. Interfaces 2023, 15, 14470−14480

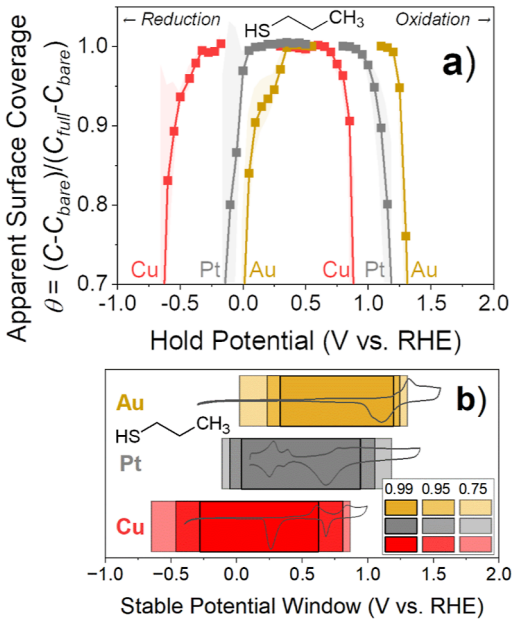

Figure 2. Electrochemical stability of C3 SAM on Au, Pt, and Cu in 0.1 M KOH after progressive two-minute potential hold experiments. (a) Average apparent surface coverage of SAM as a function of hold potential. Shaded error bars indicate the standard deviation of two experiments. (b) Potential to reach a given apparent surface coverage, θ, on each metal determined by linear interpolation of (a).

shows linearly interpolated potentials corresponding to different apparent surface coverages (θ = 0.99, 0.95, 0.75) based on the data in Figure 2a. This provides a practical guide for estimating C3 SAM surface coverage under different electrochemical conditions.

C3 maintains a saturating monolayer (θ = 1) on Au until around 0.33 V versus RHE, which agrees with the reductive desorption CV in Figure 1. The dip in coverage to around θ = 0.85, before θ decreases rapidly to zero (left Au trace in Figure 2a), corresponds to the first desorption peak in Figure 1, representing removal of the SAM from lower coordinated Au sites.[20] In comparison, the reductive traces of Pt and Cu do not show this feature. Pt maintains full coverage down to about 0.02 V versus RHE, while Cu does not lose coverage until −0.33 V versus RHE. This is correlated with the potential for HER onset on both surfaces, suggesting that hydrogen adsorption may play a role. The reductive stability has the order Au < Pt < Cu and qualitatively agrees with what has been found previously in the literature.[8,10,11,29−31]

The reductive desorption trends can be partially understood by the binding strength of sulfur with each surface, as the mechanism in basic conditions is believed to be simple one-electron transfer, leading to a solution phase thiolate.[8] However, while Au does bind sulfur the most weakly,[10,11] sulfur binds to Pt more strongly than Cu.[32] This latter observation would predict the opposite trend from what we see in Figure 2, where the thiolates are more stable on Cu than Pt. One likely reason is that Pt adsorbs hydrogen at higher potentials than Cu.[33] The adsorbed hydrogen may play a role in desorption of the thiolate from the surface, either by driving the formation of the thiol (R−SH) or by simply exhibiting competitive adsorption.[34] Direct thiol formation is only expected for pH < thiol pK_a (~10−11), so we suspect in the present example that competitive adsorption is dominant. It is worth noting that surface reconstruction occurs due to thiolate SAM formation on Au[34−36] and Cu[6,30,36,37] (while there is no evidence of such a process on Pt[36]); this may also play a role in SAM stability differences across metals.

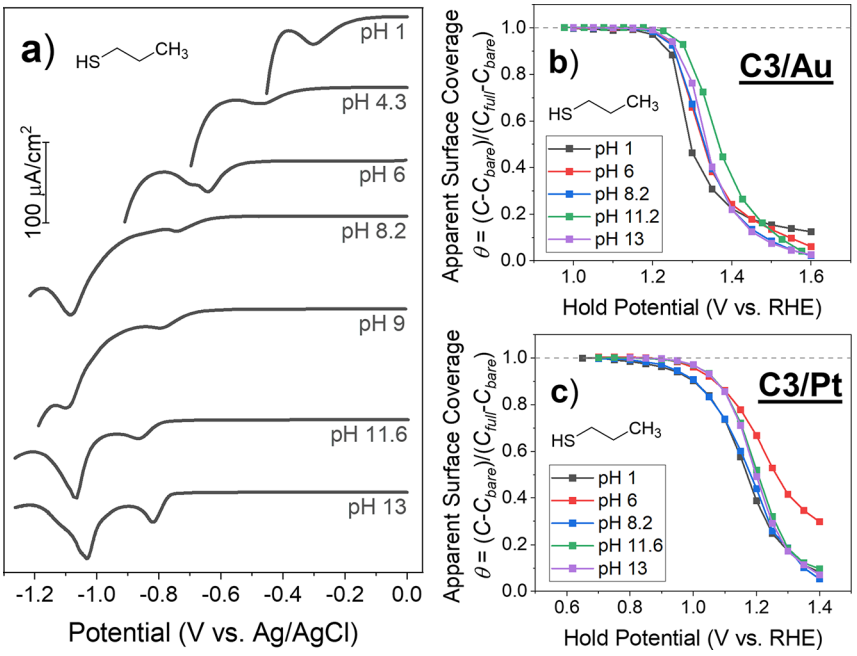

Figure 3. C3 desorption as a function of pH (1: $HClO_4$; 4.3: NaH_2PO_4; 6: NaH_2PO_4 and Na_2HPO_4; 8.2: $NaHCO_3$; 9: Na_2HPO_4; 11.6: Na_2CO_3; 13: KOH). (a) Reductive desorption LSVs of C3 from Au at 100 mV/s. (b) Apparent surface coverages of SAM, θ, for the oxidative desorption of C3 from Au vs two-minute hold potential. (c) Apparent surface coverages of SAM, θ, for the oxidative desorption of C3 from Pt vs two-minute hold potential.

https://doi.org/10.1021/acsami.3c01224
ACS Appl. Mater. Interfaces 2023, 15, 14470−14480

The oxidative desorption traces (right in Figure 2a) for Au, Pt, and Cu all have similar shapes with $\theta = 1$ maintained up to approximately 1.20, 0.95, and 0.71 V versus RHE, respectively. There is little data on the oxidation of thiols for comparison, though desorption from Au agrees with other reports at this pH.[8] Oxidative stability has the order Au > Pt > Cu. This trend is correlated with the binding strength of oxygen,[32] supporting the idea that both thiol oxidation and surface oxidation require co-adsorption of oxygen on the surface.

3.3. Effect of pH. Next, continuing with C3 as a model SAM, the influence of electrolyte pH was investigated. The pH was varied between 1 and 13, and Cu was not studied due to its tendency to dissolve in acidic solutions. Despite discontinuing the investigation of Cu, we expect the pH trends found on Au and Pt to generally hold on Cu (at pHs where Cu does not dissolve) since pH-dependent oxidation and protonation/deprotonation of thiols should be independent of the metal. Reductive desorption of C3 from Au is shown in Figure 3a. At high pH (13 and 11.6), the LSVs are nearly identical, showing the two characteristic desorption peaks from different facets. At progressively lower pHs, from 9 to 1, the first desorption peak shifts to more positive potentials. This pH-dependent reductive desorption has also been observed for 1-nonanethiol on Au(111).[38] This is most likely due to the increased ability for proton abstraction from water (or increased proton concentration) with decreasing pH, allowing the sulfur atom to acquire a proton and desorb from the surface as a thiol. This pH dependence only occurs when the thiol is protonated (pH < pK_a), and in this regime, the desorption peak potential varies near to the expected Nernstian shift of −59 mV/pH unit (Figure S5a). Solubility of the desorbed species cannot explain the pH-dependent reductive desorption behavior since the ionic molecule is more soluble in water than the neutral analogue, and that would predict earlier desorption for pH > pK_a.

The pH dependence of the oxidative stability of C3 on Au (Figure 3b) and Pt (Figure 3c) was investigated using additional potential hold experiments. The apparent SAM coverage plotted against the hold potential shows that the oxidative desorption behavior of C3 on Au and Pt is largely invariant on the RHE scale. Figure S5b shows that the potential to achieve $\theta = 0.95$ varies linearly with slopes close to −59 mV (vs Ag/AgCl) per pH unit for both Au and Pt. This is consistent with what has been found on Au previously by Widrig et al. investigating oxidation peak potentials of C3/Au at different pHs.[8] Deviations from the exact RHE relationship could be attributed to scatter from independent measurements at each pH, different anions at each pH, or differences in unmodified metal capacitance versus pH, while SAM capacitance remains more constant (Figures S6a,b and S7). Nevertheless, we can conclude that C3 begins to be oxidized and desorbed ($\theta \sim 0.95$) in the range of 1.2−1.25 V versus RHE on Au and 0.9−1.05 V versus RHE on Pt.

3.4. Effect of Thiol. Thiols with a variety of tail structures and chemistries were next investigated to identify trends between SAM properties and their electrochemical stability and behavior. Different thiols were compared on Au versus Pt to gain a basic understanding of whether the role of underlying metal composition can differ from what was identified with C3 in Section 3.1. Cu was not further investigated due to measurement variability, especially for thiols with functional groups. Surface oxides formed on Cu when exposed to basic electrolytes (to obtain unmodified Cu C_{dl}) and/or air, and thiols are known to reduce Cu oxides to metallic Cu and form dithiol byproducts. In addition, unlike Au and Pt, there is not an abundance of single crystal STM literature to guide the understanding of the interplay of structures, surface reconstruction, and electrochemical stability of different SAMs on Cu.

First, alkanethiols were investigated to identify trends in desorption behavior as a function of carbon chain length. As shown in Figure 4a, on Au, the reductive desorption LSV peaks

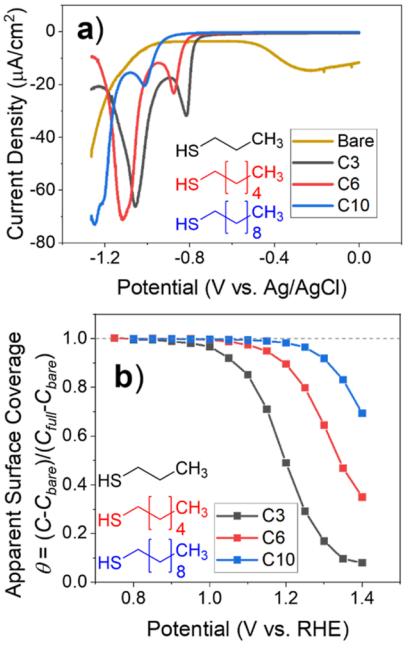

Figure 4. Reductive and oxidative stability of C3, C6, and C10 in 0.1 M KOH. (a) Cyclic voltammetry at 100 mV/s showing reductive desorption of alkanethiols on Au compared to unmodified Au. (b) SAM apparent surface coverage at different two-minute hold potentials showing oxidative desorption for alkanethiols on Pt.

shift to more negative potentials with increasing chain length, consistent with stronger lateral interactions per molecule between longer chains.[8] Water (and solvated cations) must diffuse through the SAM to reach the electrode surface and replace the space vacated by the desorbing thiolates; consequently, the reductive desorption of thiolates is often written as a solvent replacement reaction.[9] Longer alkanethiolates leave hydrophobic vacancies that repel water and ions. Exceptions to these considerations may be possible—for example, Pd surfaces can form a PdS interlayer that makes intra-SAM interactions less important[39]—but no such behaviors are documented for the metals studied here.

Next, oxidative desorption is shown as a function of carbon chain length for Pt electrodes in Figure 4b. This shows an analogous chain length dependence to the trends seen in reductive desorption. Each desorption curve has similar shape but is shifted in potential based on the chain length. Even though the mechanism of oxidation is different and requires oxygen-addition steps, the same arguments can be made that thicker SAMs (longer thiolates) have lower permeability to water and ions and require a larger driving force for oxidative desorption. SAM order or crystallinity can also play a role in the observed stability,[8] as shorter alkanethiolate SAMs are less ordered than longer chain ones (c.f. contact angle measurements in Figure S3).

https://doi.org/10.1021/acsami.3c01224
ACS Appl. Mater. Interfaces 2023, 15, 14470−14480

In contrast to alkanethiols, functionalized thiols have different molecular interactions and consequently different adsorbate structures and electrochemical behaviors. These are also the most likely thiols to be used to target specific intermolecular interactions with other species, such as for sensing or catalysis applications. The stable potential window (recorded for θ = 0.95 and 0.99 from potential hold experiments as described earlier) for a variety of thiols on Au and Pt is shown in Figure 5. Comparisons to the model C3 SAM system are used to help explain differences in thiol stability windows below.

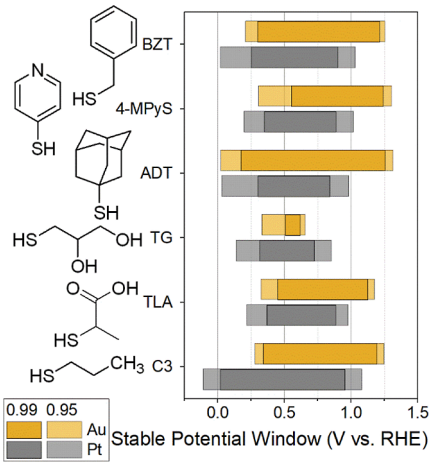

Figure 5. Electrochemical stability window of different thiols on Au and Pt in 0.1 M KOH (based on the linearly interpolated hold potential required to reach 95 and 99% apparent surface coverage, θ, from two-minute hold experiments).

First, aromatic thiols are discussed. Benzylmercaptan (BZT) is found to be more reductively stable than C3 on Au (Figure 5). Reductive desorption curves shown in Figure 6a further illustrate this observation (estimated surface coverages and peak potentials of all curves in Figure 6 are reported in Figures S8 and S9). The increased stability of BZT is probably due to BZT forming a thicker SAM that retards the diffusion of solvents, as BZT molecules have been shown to reconstruct the Au surface and orient upright to maximize stabilizing intermolecular interactions.[40] In contrast, BZT/Pt is less reductively stable than C3/Pt. BZT SAMs on Pt have been found to have less long-range order than BZT on Ag[41] (which reconstructs, like Au, to improve ordering[36]). Unlike on Au, BZT molecules on Pt orient their aromatic rings more parallel to the surface,[42] presumably resulting in a smaller film thickness. At the same time, C3 films on both surfaces have relatively similar upright configurations.[18,36,41] These inferences are supported by capacitance measurements, which show a reversal effect: C3/Au > BZT/Au and C3/Pt < BZT/Pt (Figure S6c). Higher capacitance can be interpreted as higher permeability to ions and water and thus correlates with electrochemical stability when comparing similar (e.g., nonpolar) molecules on the same metal. While the film ordering may thus explain the stability trend, another difference between Au and Pt to acknowledge is the role of hydrogen adsorption on Pt. There should be a similar driving force for this process through either C3 or BZT SAMs (forming Pt−H bond in either case, with hydrophobicity minimizing interactions between the adsorbed hydrogen and water);

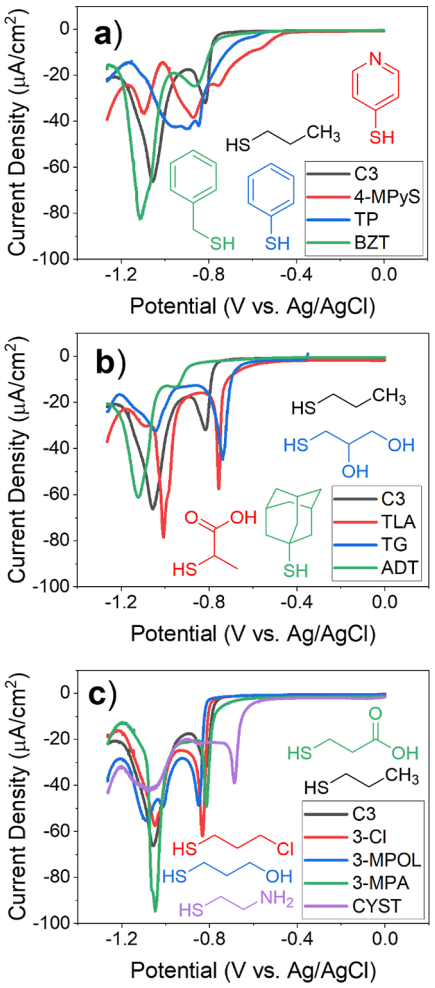

Figure 6. Linear sweep voltammetry at 100 mV/s showing reductive desorption of (a) aromatic, (b) non-aromatic branched, and (c) linear thiols with different tail groups, on Au in 0.1 M KOH, compared to C3 (black trace on all).

however, the more disordered BZT SAM could lend itself to more kinetically favorable hydrogen adsorption. This could amplify the instability of BZT/Pt but only presuming that the disorder effect is also at play. In sum, surface reconstruction on Au appears to enable more upright and stabilizing intermolecular interactions of BZT molecules, in contrast to Pt.

On both Au and Pt, 4-mercaptopyridine (4-MPyS) is much less reductively stable than C3 (Figure 5). This could possibly be explained by the pyridinic nitrogen hydrophilicity enhancing the transport of ions to the electrode surface. However, the complex reductive desorption features observed on Au in Figure 6a suggest a more elaborate behavior. In particular, pyridine is electrochemically active on Au and can pick up a proton to form pyridinium, which can be reduced in a one-electron transfer reaction.[43] This apparently destabilizes the SAM.

Thiophenol (TP) has a reductive stability that is intermediate between 4-MPyS and BZT based on the LSVs in Figure 6a. TP does not have the destabilizing influence of pyridine reduction like 4-MPyS, but the lower reductive stability of TP compared to BZT can likely be attributed to lower SAM thickness and weaker intermolecular interactions.[40,44]

https://doi.org/10.1021/acsami.3c01224
ACS Appl. Mater. Interfaces 2023, 15, 14470−14480

Oxidatively, 4-MPyS and BZT are of similar or slightly greater stability than C3 on Au (Figure 5). 4-MPyS has been shown to arrange itself in a striped phase on Au(111),[45] and it has been suggested that BZT forms an adlayer similar to that of alkanethiols on Au(111), oriented perpendicular to the surface.[40] Despite adopting stabilizing configurations that promote $\pi-\pi$ (ring-stacking) interactions and most likely having a greater SAM thickness than C3, the surface accessibility (free surface atom density) of these SAMs may be greater than for C3 and offset the stabilizing influence of the SAM thickness. Unlike the behavior of Au, 4-MPyS and BZT are less oxidatively stable than C3 on Pt. As mentioned above when discussing their reductive stability, BZT molecules on Pt do not induce reconstruction, and they orient their aromatic rings more parallel to the surface,[42] presumably resulting in a smaller film thickness compared to Au. Related differences in restructuring likely explain the lower stability of 4-MPyS (relative to C3) on Pt as well. In addition, if the pyridinic nitrogen is oriented closer to the Pt surface than on Au, it may facilitate desorption through interactions with water and ions. Thus, differences in SAM structure, orientation, and surface restructuring may contribute to differences in the relative oxidative stability of aromatic thiols versus C3 on Au and Pt.

Next, non-aromatic thiols with various functionalities were investigated. Thiolactic acid (TLA) is less stable than C3 both reductively and oxidatively on both Au and Pt (Figures 5 and 6b). This observation can be understood from several contributions. First, the packing of a TLA SAM is much different than that of an alkanethiolate SAM. The branching of the carbon connected to the sulfur creates a less compact arrangement, resulting in a lower surface coverage[46] than C3 (Figure S8a) due to steric hindrance, and providing greater defects for initiating SAM removal.[23] In addition, the hydrophilic carboxylic acid groups of TLA can more easily shuttle water and ions than methylene groups can in an alkanethiol. Also, a TLA SAM presumably has a lower effective film thickness than C3, decreasing the distance that ions and H_2O must permeate through from the bulk solution.

Thioglycerol (TG) also has lower oxidative and reductive stability on both Au and Pt compared to C3 (Figure 5). This is again most likely due to the hydrophilicity of the TG SAM as well as lower packing density than C3[47] (Figure S8a). For reduction, the hydrophilic TG molecules can promote the desorptive solvent−replacement reaction and/or hydrogen abstraction from water. For oxidation, TG molecules similarly can allow water or OH^- to reach the surface and oxidize the thiol more easily. TG is even less oxidatively stable than TLA despite it possibly forming a thicker SAM with stronger intermolecular interactions; this suggests that a more complex behavior may be occurring, such as oxidation of the OH groups (further illustrated in Figure S10).

Adamantanethiol (ADT/Au) is more stable than C3/Au (Figures 5 and 6b). Since hydrogen adsorbs very weakly (if at all) on Au,[33] the position of reductive desorption peaks on Au is more directly related to the SAM thickness (based on the chain-length dependence of alkanethiols) and strength of lateral interactions between adjacent molecules (which must be broken to allow water and cations to reach the surface). Since ADT shows higher stability than C3, the film thickness apparently outweighs the destabilizing influence of weaker lateral interactions and defects.[48−50] The greater oxidative stability of ADT can be explained in the same way.

ADT/Pt is less stable than C3/Pt (Figure 5). This is opposite to what was observed on Au.[49] ADT has lower surface coverage than C3 (Figure S8a) and greater defect density due to non-ideal packing of the bulky tail group. For the reductive stability, the greater defect density can enhance co-adsorption of hydrogen to destabilize ADT on Pt. This argument does not alone differentiate the situations on Pt and Au, since ADT has lower density than C3 on both, but thiols exposed to Pt do not induce reconstruction, while on Au, ADT molecules induce reconstruction with a significant population of Au adatoms bound to the sulfur groups.[48] Bulkier thiols TP, BZT, and 4-MPyS on Pt have generally been observed to be less ordered than their Au and Ag counterparts.[41] In addition, short chain alkanethiols on Pt are less ordered than their counterparts on Au[28] (Figures S3 and S6). The lack of surface reconstruction on Pt may prevent the formation of more ordered SAM structures like their counterparts on Au. Therefore, ADT, BZT, and 4-MPyS are all observed to be less stable than C3 on Pt, while they are of similar stability to C3 on Au.

Finally, the reductive desorption behavior of linear thiols with different terminal functional groups was investigated on Au using LSV in Figure 6c. The three-carbon SAMs (3-MPA, 3-MPOL, 3-Cl, and C3) all have similar stability (first reductive desorption peaks within 30 mV of each other). The carboxylic acid terminated SAM (3-MPA) is slightly less stable than the other three-carbon SAMs (demonstrated by an earlier and broader first peak onset), likely due to electrostatic repulsion of the carboxylates[51] and decrease in the stabilizing hydrophobic intermolecular interactions of the methylene spacer chain. The broader first peak onset mirrors the one for TLA (which also has a carboxyl group) in Figure 6a. The other three-carbon SAMs exhibit stability in the order C3 ≤ 3-Cl ≤ 3-MPOL. Nevertheless, the similarity in stabilities of these four SAMs demonstrates that, at least for linear three-carbon thiols with different small tail groups, the electrochemical stability is largely dictated by the film thickness (distance of end group from the surface), and with comparable surface coverages (Figure S8a), defects will play less of a role. On the other hand, cysteamine (CYST) was also investigated and found to be much less stable than the three-carbon thiols. It has been previously noted that each carbon in a linear alkanethiol adds about 20 mV of reductive stability;[8] here, the two-carbon amine-terminated thiol (CYST) is less stable than the three-carbon thiols by almost 200 mV, suggesting other effects play a role. One possibility is the disorder of such a short SAM,[8] and related is the ability for the amine group to interact with the metal surface and adopt a more flat-lying conformation,[52] which could help explain its lower surface coverage (Figure 6a). The amine group can also provide hydrophilic intermolecular interactions with water and cations close to the surface facilitating desorption.

In summary, differences in SAM hydrophilicity, orientation, adsorbate structures, coverage, and surface reconstruction can affect the electrochemical stability of thiols on different metals. Hydrophilic groups generally reduce electrochemical stability by enhancing diffusion of water and ions to the electrode surface compared to their alkanethiol counterparts. On Au, different tail groups on a linear thiol have a minor effect on the stability; SAM thickness is a better predictor. On Pt, non-alkanethiol SAMs are generally less stable than a similar chain length alkanethiol, presumably due to the lack of surface reconstruction, which results in a less ordered SAM with

https://doi.org/10.1021/acsami.3c01224
ACS Appl. Mater. Interfaces 2023, 15, 14470−14480

greater population of defects (compared to Au), allowing access for competitive adsorption by hydrogen or oxygen.

3.5. Consequences for Electrochemical Applications of SAMs. From this work, it can be concluded that reactions requiring extreme reducing or oxidizing potentials are unlikely to be run within the potential stability window of common SAM-metal systems. The best candidate reactions will generally be those that occur within the thermodynamic stability window of water and include high potential reductions (e.g., reduction of O_2 to water or hydrogen peroxide) or low potential oxidations (e.g., oxidations of H_2 or organic molecules such as formic acid or methanol). These reactions are commonly encountered in galvanic systems such as fuel cells and in very mild electrosynthetic applications (e.g., conversion of aldehydes to acids[53,54]). Conversely, reactions such as CO_2RR, N_2 reduction, and water splitting are less ideal candidates, although they can be accessible on SAM materials that promote the reactions with very small overpotentials. For example, conversion of CO_2 to CO is often achievable on Au catalysts near 0 V.[55] Other CO_2RR products tend to require larger overpotentials, but it is possible that those could be lowered with an appropriate SAM. Table 1 lists some common reactions with a summary of their prospects for mediation by thiolate SAMs based on our analysis of the findings in this work.

Table 1. Some Common Reactions and Their Viability for the Application of Thiolate SAMs[a,b]

reaction	E^0 (V)	viability for reduction reaction	viability for oxidation reaction
$CO_{2(g)} + 2H^+ + 2e^- \leftrightarrow CO_{(g)} + H_2O$	−0.10	?[4,61−64]	?
$CO_{2(g)} + 2H^+ + 2e^- \leftrightarrow HCOOH$	−0.11	?[62,63]	√[45,60]
$2H^+ + 2e^- \leftrightarrow H_{2(g)}$	0.00	? [65]	√ [66]
$CO_{2(g)} + 6H^+ + 6e^- \leftrightarrow CH_3OH + H_2O$	0.02 [67]	?	√
$N_{2(g)} + 8H^+ + 6e^- \leftrightarrow 2NH_4^+$	0.27	?	√
$2CO_{2(g)} + 12H^+ + 12e^- \leftrightarrow CH_3CH_2OH + 3H_2O$	0.08 [67]	?[30,63]	√
$CO_{2(g)} + 8H^+ + 8e^- \leftrightarrow CH_{4(g)} + 2H_2O$	0.17	? [61]	?
$HNO_2 + 7H^+ + 6e^- \leftrightarrow NH_4^+ + 2H_2O$	0.86	?	?
$NO_3^- + 10H^+ + 8e^- \leftrightarrow NH_4^+ + 3H_2O$	0.88	?	?
$O_{2(g)} + 2H^+ + 2e^- \leftrightarrow H_2O_2$	0.70	√ [68]	? [69]
$O_{2(g)} + 4H^+ + 4e^- \leftrightarrow 2H_2O$	1.23	√[56−58]	×

[a]Standard potentials, E^0, versus SHE, from ref[70] unless otherwise noted. [b]Legend: √: thiolate SAMs stable over the entire potential range; ?: depends on catalyst, thiol, and electrolyte or could obtain stable partial coverages; ×: unstable (for OER, thiols do not bind to metal oxides). Reference numbers next to ? or √ indicate literature examples of thiolate SAMs for that system.

For reactions that occur safely within most SAM stability windows, there are numerous examples of successful applications of SAM surface modification. One example is the selective ORR, where the reduction of O_2 to H_2O_2 over H_2O is desired. Studies investigating the effect of thiolate ligands on Au and Pt nanoparticles for ORR have found differences in overpotential, stability, and selectivity depending on particle size and ligand surface coverage.[56−58] Evidence has also been shown that ligands can electronically modify the surface and alter the intrinsic ORR activity of the metal sites.[59] Another example of the successful application of SAMs is in the formic acid oxidation reaction, where 4-MPyS SAMs on Au and Pt have been shown to increase activity.[45,60] Hermann and co-workers have proposed that surface bound 4-MPyS prevents active Au sites from being poisoned by an unfavorable binding orientation of formates. Deng and colleagues also found a benefit of using 4-MPyS modification on Pt due to the pyridinic nitrogen acting as a proton acceptor.

Despite most studies of CO_2RR operating at potentials below the onset of SAM desorption, the use of SAMs for this reaction has been demonstrated for suppression of HER in favor of CO_2 reduction due to the creation of a hydrophobic microenvironment. As may be expected, however, thiolate coverage is generally reported to decrease with electrolysis time. For example, glutathione ligands on Cu were shown to greatly increase Faradaic efficiency toward methane over hydrogen when compared to unmodified Cu; although stability tests showed a loss of hydrophobicity, Faradaic efficiency toward methane only slightly decreased from 55 to 40% (unmodified Cu produced minimal methane) and XPS showed well-formed Cu−S and N−H (indicative of glutathione) peaks, demonstrating persistent surface modification after a 7 h electrolysis at 100 mA/cm^2.[62] Another study showed that dodecanethiol-modified Au nanoparticles act like a selectively permeable film for CO_2, preventing the deposition of trace metal ion electrolyte contaminants that would otherwise poison the catalyst surface.[4] Despite reporting a greater than 75% dodecanethiol loss after a 2 h electrolysis at −1.1 V versus RHE, researchers found that 85% of the initial activity still remained. These examples demonstrate that even with some ligand loss, a partial coverage SAM may still achieve desirable catalytic effects. These partial coverage SAMs may be inhomogeneous, meaning that they remain dense (stabilized by lateral interactions) on some surface facets, or they may manifest with less dense structures strongly bound to certain surface site types. Assigning thiolate desorption from a specific facet or site type can require detailed and challenging characterization studies, but these examples suggest that with proper optimization, it may be possible to selectively (and stably) block certain active sites while leaving others free.

Another approach to form a selectively thiolated surface is the partial desorption of thiolates prior to reaction. This is possible when the thiolates have large enough differences in their binding strengths on different surface facets. This concept has been leveraged on polycrystalline Au, where ORR was selectively conducted on Au(111) by desorption of thiolates from Au(111) at a potential that maintained SAMs on the lower coordinated Au sites [i.e., Au(110) and Au(100)].[68] In another study, a polycrystalline Au surface was similarly prepared with cysteine selectively blocking Au(110) and Au(100) sites.[69] The accessible Au(111) sites were used to detect H_2O_2 in alkaline media at low concentrations. Enhanced H_2O_2 oxidation was attributed to the Au surface gaining a partial positive charge from the cysteine modification. Pretreatment to a stable partial coverage could thus be an option to eliminate dynamic catalytic behavior and provide more confidence in mechanistic studies of SAM-mediated reactions.

The examples in this section demonstrate a variety of situations where SAMs can be electrochemically stable and provide a beneficial effect (e.g., reduce electrode poisoning, create a hydrophobic near-surface environment, promote

https://doi.org/10.1021/acsami.3c01224
ACS Appl. Mater. Interfaces 2023, 15, 14470−14480

interfacial chemistry, etc.). It is also critical to consider stability over long-term applications. Researchers should be wary of dynamic catalytic effects when operating at potentials near the edge of the SAM stability window. Long electrolysis times may lead to gradual desorption or degradation of the SAM, and this could manifest in complex ways, such as in differential breakdown or desorption at one site type relative to another.[30,63] Strategies can be undertaken to increase the stability of SAM-metal systems such as electrolyte engineering, the use of longer chain ligands, the use of metals that bind sulfur more strongly, or the implementation of cross-linked or multidentate SAMs. Nevertheless, this discussion highlights the importance of surface characterization before and after reaction. Coverage losses should be assessed in detail (before and after reaction), through double layer capacitance as well as more direct techniques such as XPS, IR, or ICP−MS/AA where available.

4. CONCLUSIONS

In conclusion, the electrochemical stability of a variety of thiols on Au, Pt, and Cu was identified in different aqueous electrolytes. The investigation of different metal, thiol, and pH combinations under a uniform measurement protocol provides valuable insights into the effects of these different variables on SAM stability to guide researchers in the electrochemical application of thiolate SAMs. For C3 as a benchmark, the reductive stability increases in the order Au < Pt < Cu, while the oxidative stability increases in the order Cu < Pt < Au. The order of reductive stability is correlated with the binding energy of sulfur, except for Pt, which gives lower stability than would be expected, due to hydrogen adsorption. The order of oxidative stability is correlated with the order of surface oxide formation (i.e., oxygen binding energy). Reductive desorption is a one-electron transfer reaction, and at pHs below the pK_a of the thiol, the reductive desorption potential increases with decreasing pH. Oxidative desorption potential increases with decreasing pH across all pHs. In general, SAMs suppress surface oxide formation and hydrogen evolution, but these processes ultimately coincide with degradation and removal of the SAM.

The electrochemical stability of specific thiols depends on many different factors including SAM surface coverage or defects, SAM thickness, intermolecular interactions from different functional groups, surface reconstruction induced by SAM formation, and the reactivity of the non-sulfur part of the SAM molecule (e.g., pyridinic nitrogen on 4-MPyS). The electrochemical stability of alkanethiols scales with the carbon chain length, which is a good predictor of the range of SAM stability versus electrochemical potential. Lower coverage and/or hydrophilic SAMs generally lower the electrochemical stability in both the oxidative and reductive directions, as they increase the ability for ions and water to reach the metal surface atoms. Deviations from these trends are due to material-specific effects. For Au, SAM thickness plays the most important role in SAM stability since surface reconstruction often allows for a more ordered structure (than Pt) which reduces the number of SAM defects. For Pt, non-alkanethiolate SAMs are generally less stable than an alkanethiolate of a similar chain length. Because of the lack of surface reconstruction on Pt, these SAMs are generally highly defective and consequently provide greater surface accessibility than equivalent SAMs on Au, allowing the adsorption of hydrogen and oxygen at reductive and oxidative potentials, respectively.

ASSOCIATED CONTENT

Supporting Information

The Supporting Information is available free of charge at https://pubs.acs.org/doi/10.1021/acsami.3c01224.

Potential hold sequences, XPS of C3 on Au at different potentials, contact angle measurements, consecutive direct desorption CVs, desorption potential versus pH, double layer capacitance measurements, comparison of low pH and high pH capacitance measurements, estimated surface coverage and peak potentials of SAMs on Au from reductive desorption curves, and apparent surface coverage of TG on Au (PDF)

AUTHOR INFORMATION

Corresponding Authors

J. Will Medlin − *Department of Chemical and Biological Engineering, University of Colorado Boulder, Boulder, Colorado 80303, United States;* orcid.org/0000-0003-2404-2443; Email: will.medlin@colorado.edu

Adam Holewinski − *Department of Chemical and Biological Engineering, University of Colorado Boulder, Boulder, Colorado 80303, United States; Renewable and Sustainable Energy Institute, University of Colorado Boulder, Boulder, Colorado 80309, United States;* orcid.org/0000-0001-8307-5881; Email: adam.holewinski@colorado.edu

Author

Nathanael C. Ramos − *Department of Chemical and Biological Engineering, University of Colorado Boulder, Boulder, Colorado 80303, United States; Renewable and Sustainable Energy Institute, University of Colorado Boulder, Boulder, Colorado 80309, United States;* orcid.org/0000-0002-4721-0350

Complete contact information is available at: https://pubs.acs.org/10.1021/acsami.3c01224

Notes

The authors declare no competing financial interest.

ACKNOWLEDGMENTS

The authors acknowledge support from the National Science Foundation (CBET 2004090). N.C.R. acknowledges support from the Graduate Assistance in Areas of National Need (GAANN) fellowship from the U.S. Department of Education.

REFERENCES

(1) Zhu, Q.; Murphy, C. J.; Baker, L. R. Opportunities for Electrocatalytic CO2 Reduction Enabled by Surface Ligands. *J. Am. Chem. Soc.* **2022**, *144*, 2829−2840.

(2) Schoenbaum, C. A.; Schwartz, D. K.; Medlin, J. W. Controlling the Surface Environment of Heterogeneous Catalysts Using Self-Assembled Monolayers. *Acc. Chem. Res.* **2014**, *47*, 1438−1445.

(3) Kahsar, K. R.; Schwartz, D. K.; Medlin, J. W. Control of Metal Catalyst Selectivity through Specific Noncovalent Molecular Interactions. *J. Am. Chem. Soc.* **2014**, *136*, 520−526.

(4) Shang, H.; Wallentine, S. K.; Hofmann, D. M.; Zhu, Q.; Murphy, C. J.; Baker, L. R. Effect of Surface Ligands on Gold Nanocatalysts for CO2 Reduction. *Chem. Sci.* **2020**, *11*, 12298−12306.

(5) Souza, M. L.; Lima, F. H. B. Dibenzyldithiocarbamate-Functionalized Small Gold Nanoparticles as Selective Catalysts for the Electrochemical Reduction of CO2to CO. *ACS Catal.* **2021**, *11*, 12208−12219.

(6) Schlenoff, J. B.; Li, M.; Ly, H. Stability and Self-Exchange in Alkanethiol Monolayers. *J. Am. Chem. Soc.* **1995**, *117*, 12528−12536.
(7) Laibinis, P. E.; Whitesides, G. M. Self-Assembled Monolayers of n-Alkanethiolates on Copper Are Barrier Films That Protect the Metal against Oxidation by Air. *J. Am. Chem. Soc.* **1992**, *114*, 9022−9028.
(8) Widrig, C. A.; Chung, C.; Porter, M. D. The Electrochemical Desorption of N-Alkanethiol Monolayers from Polycrystalline Au and Ag Electrodes. *J. Electroanal. Chem.* **1991**, *310*, 335−359.
(9) Salvarezza, R. C.; Carro, P. The Electrochemical Stability of Thiols on Gold Surfaces. *J. Electroanal. Chem.* **2018**, *819*, 234−239.
(10) Floridia Addato, M. A.; Rubert, A.; Benítez, G.; Zelaya, E.; Cabello, G.; Cuesta, A.; Thomas, J. E.; Visintín, A.; Salvarezza, R. C.; Fonticelli, M. H. Electrochemical Desorption of Thiolates and Sulfur from Nanoparticle and Planar Platinum Surfaces. *J. Phys. Chem. C* **2013**, *117*, 7589−7597.
(11) Azzaroni, O.; Vela, M. E.; Fonticelli, M.; Benítez, G.; Carro, P.; Blum, B.; Salvarezza, R. C. Electrodesorption Potentials of Self-Assembled Alkanethiolate Monolayers on Copper Electrodes. An Experimental and Theoretical Study. *J. Phys. Chem. B* **2003**, *107*, 13446−13454.
(12) Oesch, U.; Janata, J. Electrochemical Study of Gold Electrodes with Anodic Oxide Films—I. Formation and Reduction Behaviour of Anodic Oxides on Gold. *Electrochim. Acta* **1983**, *28*, 1237−1246.
(13) Strmcnik, D.; Tripkovic, D.; van der Vliet, D.; Stamenkovic, V.; Marković, N. M. Adsorption of Hydrogen on Pt(1 1 1) and Pt(1 0 0) Surfaces and Its Role in the HOR. *Electrochem. Commun.* **2008**, *10*, 1602−1605.
(14) Kuhl, K. P.; Cave, E. R.; Abram, D. N.; Jaramillo, T. F. New Insights into the Electrochemical Reduction of Carbon Dioxide on Metallic Copper Surfaces. *Energy Environ. Sci.* **2012**, *5*, 7050−7059.
(15) Nitopi, S.; Bertheussen, E.; Scott, S. B.; Liu, X.; Engstfeld, A. K.; Horch, S.; Seger, B.; Stephens, I. E. L.; Chan, K.; Hahn, C.; Nørskov, J. K.; Jaramillo, T. F.; Chorkendorff, I. Progress and Perspectives of Electrochemical CO2 Reduction on Copper in Aqueous Electrolyte. *Chem. Rev.* **2019**, *119*, 7610−7672.
(16) Love, J. C.; Estroff, L. A.; Kriebel, J. K.; Nuzzo, R. G.; Whitesides, G. M. Self-Assembled Monolayers of Thiolates on Metals as a Form of Nanotechnology. *Chem. Rev.* **2005**, *105*, 1103−1170.
(17) Diao, P.; Guo, M.; Tong, R. Characterization of Defects in the Formation Process of Self-Assembled Thiol Monolayers by Electrochemical Impedance Spectroscopy. *J. Electroanal. Chem.* **2001**, *495*, 98−105.
(18) Lang, P.; Mekhalif, Z.; Rat, B.; Garnier, F. Self-Assembled Alkylthiols Monolayers onto Platinum; Influence of the Adsorbed Oxygen. *J. Electroanal. Chem.* **1998**, *441*, 83−93.
(19) Dilimon, V. S.; Denayer, J.; Delhalle, J.; Mekhalif, Z. Electrochemical and Spectroscopic Study of the Self-Assembling Mechanism of Normal and Chelating Alkanethiols on Copper. *Langmuir* **2012**, *28*, 6857−6865.
(20) Walczak, M. M.; Alves, C. A.; Lamp, B. D.; Porter, M. D. Electrochemical and X-Ray Photoelectron Spectroscopic Evidence for Differences in the Binding Sites of Alkanethiolate Monolayers Chemisorbed at Gold. *J. Electroanal. Chem.* **1995**, *396*, 103−114.
(21) Hobara, D.; Miyake, K.; Imabayashi, S. I.; Niki, K.; Kakiuchi, T. In-Situ Scanning Tunneling Microscopy Imaging of the Reductive Desorption Process of Alkanethiols on Au(111). *Langmuir* **1998**, *14*, 3590−3596.
(22) Wano, H.; Uosaki, K. In Situ, Real-Time Monitoring of the Reductive Desorption Process of Self-Assembled Monolayers of Hexanethiol on Au(111) Surfaces in Acidic and Alkaline Aqueous Solutions by Scanning Tunneling Microscopy. *Langmuir* **2001**, *17*, 8224−8228.
(23) Luo, M.; Frechette, J. Electrochemical Stability of Low-Density Carboxylic Acid Terminated Monolayers. *J. Phys. Chem. C* **2010**, *114*, 20167−20172.
(24) Chen, Y.; Yang, C.; Wang, F.-B. Electrochemical Assessment of Electrochemical Oxidation Stability of Self-Assembled Monolayers on Gold and Preparation of Binary Self-Assembled Monolayers on Gold. *Electrochim. Acta* **2010**, *55*, 3951−3956.
(25) Hagenström, H.; Schneeweiss, M. A.; Kolb, D. M. Modification of a Au(111) Electrode with Ethanethiol. 1. Adlayer Structure and Electrochemistry. *Langmuir* **1999**, *15*, 2435−2443.
(26) Yang, D. F.; Al-Maznai, H.; Morin, M. Vibrational Study of the Fast Reductive and the Slow Oxidative Desorptions of a Nonanethiol Self-Assembled Monolayer from a Au(111) Single Crystal Electrode. *J. Phys. Chem. B* **1997**, *101*, 1158−1166.
(27) Schwartz, D. K. Mechanisms and Kinetics of Self-Assembled Monolayer Formation. *Annu. Rev. Phys. Chem.* **2001**, *52*, 107−137.
(28) Floridia Addato, M. A.; Rubert, A. A.; Benítez, G. A.; Fonticelli, M. H.; Carrasco, J.; Carro, P.; Salvarezza, R. C. Alkanethiol Adsorption on Platinum: Chain Length Effects on the Quality of Self-Assembled Monolayers. *J. Phys. Chem. C* **2011**, *115*, 17788−17798.
(29) Azzaroni, O.; Vela, M. E.; Andreasen, G.; Carro, P.; Salvarezza, R. C. Electrodesorption Potentials of Self-Assembled Alkanethiolate Monolayers on Ag(111) and Au(111). An Electrochemical, Scanning Tunneling Microscopy and Density Functional Theory Study. *J. Phys. Chem. B* **2002**, *106*, 12267−12273.
(30) Iijima, G.; Yamaguchi, H.; Inomata, T.; Yoto, H.; Ito, M.; Masuda, H. Methanethiol SAMs Induce Reconstruction and Formation of Cu+ on a Cu Catalyst under Electrochemical CO2 Reduction. *ACS Catal.* **2020**, *10*, 15238−15249.
(31) DeLeon, M.; Baldelli, S. Electroreductive Desorption of Alkanethiols on Gold and UPD Copper/Gold Surfaces Using In Situ Second Harmonic Generation. *J. Electrochem. Soc.* **2020**, *167*, 166519.
(32) Abild-Pedersen, F.; Greeley, J.; Studt, F.; Rossmeisl, J.; Munter, T. R.; Moses, P. G.; Skúlason, E.; Bligaard, T.; Nørskov, J. K. Scaling Properties of Adsorption Energies for Hydrogen-Containing Molecules on Transition-Metal Surfaces. *Phys. Rev. Lett.* **2007**, *99*, 016105.
(33) Greeley, J.; Jaramillo, T. F.; Bonde, J.; Chorkendorff, I.; Nørskov, J. K. Computational High-Throughput Screening of Electrocatalytic Materials for Hydrogen Evolution. *Nat. Mater.* **2006**, *5*, 909−913.
(34) Kautz, N. A.; Kandel, S. A. Alkanethiol/Au(111) Self-Assembled Monolayers Contain Gold Adatoms: Scanning Tunneling Microscopy before and after Reaction with Atomic Hydrogen. *J. Am. Chem. Soc.* **2008**, *130*, 6908−6909.
(35) Molina, L. M.; Hammer, B. Theoretical Study of Thiol-Induced Reconstructions on the Au(1 1 1) Surface. *Chem. Phys. Lett.* **2002**, *360*, 264−271.
(36) Vericat, C.; Vela, M. E.; Corthey, G.; Pensa, E.; Cortés, E.; Fonticelli, M. H.; Ibañez, F.; Benitez, G. E.; Carro, P.; Salvarezza, R. C. Self-Assembled Monolayers of Thiolates on Metals: A Review Article on Sulfur-Metal Chemistry and Surface Structures. *RSC Adv.* **2014**, *4*, 27730−27754.
(37) Driver, S. M.; Woodruff, D. P. Adsorption Structures of 1-Octanethiol on Cu(111) Studied by Scanning Tunneling Microscopy. *Langmuir* **2000**, *16*, 6693−6700.
(38) Yang, D. F.; Wilde, C. P.; Morin, M. Electrochemical Desorption and Adsorption of Nonyl Mercaptan at Gold Single Crystal Electrode Surfaces. *Langmuir* **1996**, *12*, 6570−6577.
(39) Corthey, G.; Rubert, A. A.; Benitez, G. A.; Fonticelli, M. H.; Salvarezza, R. C. Electrochemical and X-Ray Photoelectron Spectroscopy Characterization of Alkanethiols Adsorbed on Palladium Surfaces. *J. Phys. Chem. C* **2009**, *113*, 6735−6742.
(40) Hallmann, L.; Bashir, A.; Strunskus, T.; Adelung, R.; Staemmler, V.; Wöll, C.; Tuczek, F. Self-Assembled Monolayers of Benzylmercaptan and p-Cyanobenzylmercaptan on Au(111) Surfaces: Structural and Spectroscopic Characterization. *Langmuir* **2008**, *24*, 5726−5733.
(41) Gui, J. Y.; Stern, D. A.; Frank, D. G.; Lu, F.; Zapien, D. C.; Hubbard, A. T. Adsorption and Surface Structural Chemistry of Thiophenol, Benzyl Mercaptan, and Alkyl Mercaptans. Comparative Studies at Ag(111) and Pt(111) Electrodes by Means of Auger Spectroscopy, Electron Energy Loss Spectroscopy, Low-Energy

https://doi.org/10.1021/acsami.3c01224
ACS Appl. Mater. Interfaces 2023, 15, 14470−14480

Electron Diffraction, and Electrochemistry. *Langmuir* **1991**, *7*, 955−963.
(42) Stern, D. A.; Wellner, E.; Salaita, G. N.; Laguren-Davidson, L.; Lu, F.; Batina, N.; Frank, D. G.; Zapien, D. C.; Walton, N.; Hubbard, A. T. Adsorbed Thiophenol and Related Compounds Studied at Pt(111) Electrodes by EELS, Auger Spectroscopy, and Cyclic Voltammetry. *J. Am. Chem. Soc.* **1988**, *110*, 4885−4893.
(43) Lucio, A. J.; Shaw, S. K. Pyridine and Pyridinium Electrochemistry on Polycrystalline Gold Electrodes and Implications for CO2 Reduction. *J. Phys. Chem. C* **2015**, *119*, 12523−12530.
(44) Wan, L. J.; Terashima, M.; Noda, H.; Osawa, M. Molecular Orientation and Ordered Structure of Benzenethiol Adsorbed on Gold(111). *J. Phys. Chem. B* **2000**, *104*, 3563−3569.
(45) Hermann, J. M.; Müller, H.; Daccache, L.; Adler, C.; Keller, S.; Metzler, M.; Jacob, T.; Kibler, L. A. Formic Acid Oxidation Reaction on Au(111) Electrodes Modified with 4-Mercaptopyridine SAM. *Electrochim. Acta* **2021**, *388*, 138547.
(46) Wang, Q.; Jiang, N.; Li, N. Electrocatalytic Response of Dopamine at a Thiolactic Acid Self-Assembled Gold Electrode. *Microchem. J.* **2001**, *68*, 77−85.
(47) Burshtain, D.; Mandler, D. The Effect of Surface Attachment on Ligand Binding: Studying the Association of Mg 2+, Ca 2+ and Sr 2+ by 1-Thioglycerol and 1,4-Dithiothreitol Monolayers. *Phys. Chem. Chem. Phys.* **2006**, *8*, 158−164.
(48) Jobbins, M. M.; Raigoza, A. F.; Kandel, S. A. Adatoms at the Sulfur-Gold Interface in 1-Adamantanethiolate Monolayers, Studied Using Reaction with Hydrogen Atoms and Scanning Tunneling Microscopy. *J. Phys. Chem. C* **2011**, *115*, 25437−25441.
(49) Dameron, A. A.; Charles, L. F.; Weiss, P. S. Structures and Displacement of 1-Adamantanethiol Self-Assembled Monolayers on Au{111}. *J. Am. Chem. Soc.* **2005**, *127*, 8697−8704.
(50) Dameron, A. A.; Mullen, T. J.; Hengstebeck, R. W.; Saavedra, H. M.; Weiss, P. S. Origins of Displacement in 1-Adamantanethiolate Self-Assembled Monolayers. *J. Phys. Chem. C* **2007**, *111*, 6747−6752.
(51) Imabayashi, S.-i.; Iida, M.; Hobara, D.; Feng, Z. Q.; Niki, K.; Kakiuchi, T. Reductive Desorption of Carboxylic-Acid-Terminated Alkanethiol Monolayers from Au(111) Surfaces. *J. Electroanal. Chem.* **1997**, *428*, 33−38.
(52) Zhang, J.; Bilīč, A.; Reimers, J. R.; Hush, N. S.; Ulstrup, J. Coexistence of Multiple Conformations in Cysteamine Monolayers on Au(111). *J. Phys. Chem. B* **2005**, *109*, 15355−15367.
(53) Wang, T.; Tao, L.; Zhu, X.; Chen, C.; Chen, W.; Du, S.; Zhou, Y.; Zhou, B.; Wang, D.; Xie, C.; Long, P.; Li, W.; Wang, Y.; Chen, R.; Zou, Y.; Fu, X. Z.; Li, Y.; Duan, X.; Wang, S. Combined Anodic and Cathodic Hydrogen Production from Aldehyde Oxidation and Hydrogen Evolution Reaction. *Nat. Catal.* **2021**, *5*, 66−73.
(54) Román, A. M.; Hasse, J. C.; Medlin, J. W.; Holewinski, A. Elucidating Acidic Electro-Oxidation Pathways of Furfural on Platinum. *ACS Catal.* **2019**, *9*, 10305−10316.
(55) Chen, Y.; Li, C. W.; Kanan, M. W. Aqueous CO2 Reduction at Very Low Overpotential on Oxide-Derived Au Nanoparticles. *J. Am. Chem. Soc.* **2012**, *134*, 19969−19972.
(56) Lu, L.; Zou, S.; Zhou, Y.; Liu, J.; Li, R.; Xu, Z.; Xiao, L.; Fan, J. Ligand-Regulated ORR Activity of Au Nanoparticles in Alkaline Medium: The Importance of Surface Coverage of Ligands. *Catal. Sci. Technol.* **2018**, *8*, 746−754.
(57) Cavaliere, S.; Raynal, F.; Etcheberry, A.; Herlem, M.; Perez, H. Direct Electrocatalytic Activity of Capped Platinum Nanoparticles toward Oxygen Reduction. *Electrochem. Solid-State Lett.* **2004**, *7*, A358.
(58) Sumner, L.; Sakthivel, N. A.; Schrock, H.; Artyushkova, K.; Dass, A.; Chakraborty, S. Electrocatalytic Oxygen Reduction Activities of Thiol-Protected Nanomolecules Ranging in Size from Au28(SR)20 to Au279(SR)84. *J. Phys. Chem. C* **2018**, *122*, 24809−24817.
(59) Zhou, Z.-Y.; Kang, X.; Song, Y.; Chen, S. Ligand-Mediated Electrocatalytic Activity of Pt Nanoparticles for Oxygen Reduction Reactions. *J. Phys. Chem. C* **2012**, *116*, 10592−10598.
(60) Deng, K. C.; Lu, Z. X.; Sun, J. J.; Ye, J. Y.; Dong, F.; Su, H. S.; Yang, K.; Sartin, M. M.; Yan, S.; Cheng, J.; Zhou, Z. Y.; Ren, B. Accelerated Interfacial Proton Transfer for Promoting Electrocatalytic Activity. *Chem. Sci.* **2022**, *13*, 10884−10890.
(61) Shi, Y.; Sun, K.; Shan, J.; Li, H.; Gao, J.; Chen, Z.; Sun, C.; Shuai, Y.; Wang, Z. Selective CO2Electromethanation on Surface-Modified Cu Catalyst by Local Microenvironment Modulation. *ACS Catal.* **2022**, *12*, 8252−8258.
(62) Fang, Y.; Flake, J. C. Electrochemical Reduction of CO2 at Functionalized Au Electrodes. *J. Am. Chem. Soc.* **2017**, *139*, 3399−3405.
(63) Pankhurst, J. R.; Iyengar, P.; Loiudice, A.; Mensi, M.; Buonsanti, R. Metal−Ligand Bond Strength Determines the Fate of Organic Ligands on the Catalyst Surface during the Electrochemical CO2 Reduction Reaction. *Chem. Sci.* **2020**, *11*, 9296−9302.
(64) Wang, Z.; Wu, L.; Sun, K.; Chen, T.; Jiang, Z.; Cheng, T.; Goddard, W. A. Surface Ligand Promotion of Carbon Dioxide Reduction through Stabilizing Chemisorbed Reactive Intermediates. *J. Phys. Chem. Lett.* **2018**, *9*, 3057−3061.
(65) Muglali, M. I.; Erbe, A.; Chen, Y.; Barth, C.; Koelsch, P.; Rohwerder, M. Modulation of Electrochemical Hydrogen Evolution Rate by Araliphatic Thiol Monolayers on Gold. *Electrochim. Acta* **2013**, *90*, 17−26.
(66) Genorio, B.; Strmcnik, D.; Subbaraman, R.; Tripkovic, D.; Karapetrov, G.; Stamenkovic, V. R.; Pejovnik, S.; Marković, N. M. Selective Catalysts for the Hydrogen Oxidation and Oxygen Reduction Reactions by Patterning of Platinum with Calix[4]Arene Molecules. *Nat. Mater.* **2010**, *9*, 998−1003.
(67) Lamy, C.; Lima, A.; LeRhun, V.; Delime, F.; Coutanceau, C.; Léger, J. M. Recent Advances in the Development of Direct Alcohol Fuel Cells (DAFC). *J. Power Sources* **2002**, *105*, 283−296.
(68) El-Deab, M. S.; Arihara, K.; Ohsaka, T. Fabrication of Au(111)-Like Polycrystalline Gold Electrodes and Their Applications to Oxygen Reduction. *J. Electrochem. Soc.* **2004**, *151*, No. E213.
(69) Dutta, A.; Hasan, M. M.; Miah, M. R.; Nagao, Y.; Hasnat, M. A. Efficient Sensing of Hydrogen Peroxide via Electrocatalytic Oxidation Reactions Using Polycrystalline Au Electrode Modified with Controlled Thiol Group Immobilization. *Electrochim. Acta* **2021**, *395*, 139217.
(70) Bratsch, S. G. Standard Electrode Potentials and Temperature Coefficients in Water at 298.15 K. *J. Phys. Chem. Ref. Data* **1989**, *18*, 1.

https://doi.org/10.1021/acsami.3c01224
ACS Appl. Mater. Interfaces 2023, 15, 14470−14480